

Instrument Science Report STIS 2005-01

A New Flux Calibration for the STIS Objective Prism

Jesús Maíz-Apellániz and Ralph C. Bohlin
March 7, 2005

ABSTRACT

We have obtained a new absolute flux calibration for the STIS objective prism that yields fluxes accurate to 1% rms in the 1300-3000 Å range relative to the fluxes measured using the first-order modes G140L and G230L. We have also re-analyzed the flux calibration for $\lambda > 3000$ Å, where the accuracies are lower. The new calibration includes separate sensitivity curves for the 1200 and 2125 Å settings as well as a time-dependent sensitivity (TDS) solution similar to (but independent of) the one derived for G230L.

Introduction

The objective prism on STIS is a dispersive element with a rather unique characteristic among HST observing modes: spectra can be acquired in a single exposure all the way from 1150 Å to the optical band. This is shown in Fig. 1, where the transformation from wavelength to pixel, as well as the dispersion relation (the inverse of the derivative of the previous function) for the STIS objective prism are shown. The objective prism can use the same slits as the STIS gratings. However, its full power is best revealed in slitless mode, where the compression of the full spectrum of a single source into a small fraction of the horizontal size of the detector can be used to simultaneously obtain spectra of several hundred sources.

Despite those characteristics, the objective prism was not used as frequently in the 7+ years of the STIS lifetime as other spectroscopic observing modes (the archive contains only 123 scientific exposures). The likely explanation is multiple: low sensitivity in the FUV compared to the G140L mode, low spectral resolution in the NUV compared to the G230L or G230LB modes, highly variable spectral resolution, and the difficulties

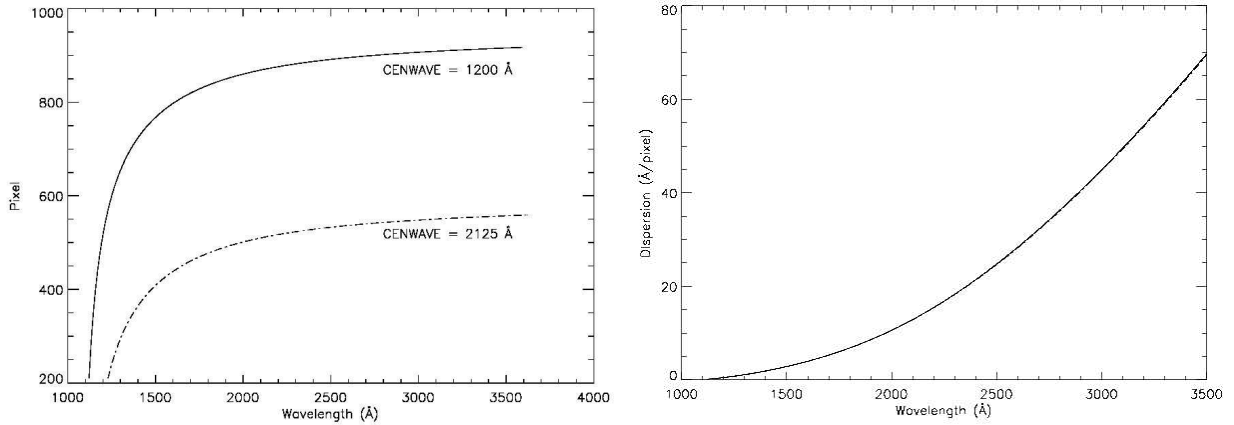


Figure 1: (left) Transformation from wavelength to pixel for the two central wavelength settings in the STIS objective prism. (right) Associated dispersion relation.

Dataset	Setting	Aperture	Date
o4pz02020	1200	52X2	21 May 1998
o4pz02030	1200	F25SRF2	21 May 1998
o68h01050	1200	52X2	18 Jul 2000
o68h01060	2125	52X2	18 Jul 2000
o8ia11050	1200	52X2	03 Sep 2002
o8ia11060	2125	52X2	03 Sep 2002
o8v540050	1200	52X2	10 Nov 2003
o8v540060	2125	52X2	10 Nov 2003

Table 1: Objective-prism datasets with observations of the standard star HS 2027+0651 used in this ISR.

inherent to dealing with crowding in slitless spectral exposures. The first two characteristics relegated the objective prism to some specific scientific tasks; the last two complications were overcome with the availability of specific software for the analysis of STIS objective-prism data (Maíz-Apellániz 2005).

Another problem is that the existing absolute flux calibration for the prism was known to be worse than that of the gratings due to the small number of spectra on which it was based. Particularly, the repeatability was rather poor. For that reason, the STIS group decided to embark on a project to produce an improved calibration and the results are presented in this Instrument Science Report.

Data and method

The datasets used for the new flux calibration of the STIS objective prism are shown in Table 1. They are all observations of the white dwarf standard HS 2027+0651. The observations cover a large fraction of the STIS lifetime (thus allowing an exploration of time-dependent effects) and were executed using the two available central wavelength settings, 1200 (5 datasets) and 2125 (3 datasets). The wide 52X2 slit was used on 7 datasets and the SRF₂ filter for the eighth. The latter cuts the spectrum below 1280 Å; however, since our analysis will concentrate on $\lambda > 1300$ Å we have also included it. Two of the exposures are shown in Fig. 2.

MULTISPEC (Maíz-Apellániz 2005) was used to extract the spectra by profile fitting in the cross-

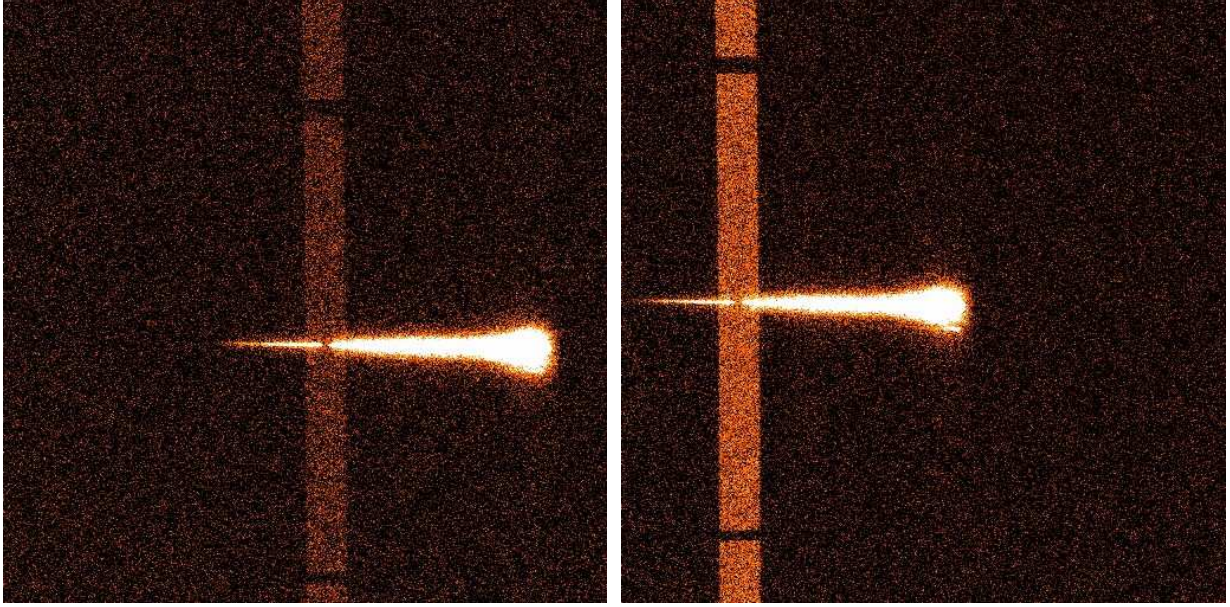


Figure 2: Two of the STIS objective-prism exposures of the standard star HS 2027+6051 used in this ISR. The left frame shows dataset o8v540060 (1200 setting) and the right frame shows dataset o8v540050 (2125 setting). The vertical band in both cases corresponds to the geocoronal Lyman α emission projected on the 52X2 slit.

dispersion direction, one column at a time. The fit residuals were found to contain 1-2% (2125 setting) or 3-5% (1200 setting) of the total flux as a result of the mismatch between the fitted profile and the real one. No significant differences were found between the residuals integrated over an 11-pixel vertical box and those integrated over a 61-pixel one. The 11-pixel residual was added to the spectra obtained by profile fitting to improve the precision of our measurements. A manual shift in the zero x position of the spectrum was applied to each dataset by comparing the FUV absorption lines with those of a reference spectrum of the same star obtained from G140L+G230L data. The obtained displacement was of the order of 1 pixel in all cases. The reason why such a shift is necessary is related to the wavelength-dependent dispersion of objective-prisms. This is illustrated in Fig. 3: if the exact zero x position is not known within better than 1 pixel, then errors of a few percent in the measured fluxes are expected for $1300 \text{ \AA} < \lambda < 3000 \text{ \AA}$. The situation is even worse at longer wavelengths, an issue that we will explore in the next section.

After the spectra were extracted, we compared the measured fluxes with those of the reference spectrum.

Results

$1300 \text{ \AA} < \lambda < 3000 \text{ \AA}$

We start by analyzing the wavelength range $1300 \text{ \AA} < \lambda < 3000 \text{ \AA}$. We plot in Fig. 4 our fluxes for each of the eight datasets divided by the reference spectrum of HS 2027+6051, i.e. the correction that needs to be applied to the sensitivity curve. Results have been rebinned onto a uniform wavelength grid and smoothed to increase the S/N ratio. There are considerable departures from unity as well as differences between different datasets. On a closer look, however, several patterns can be seen:

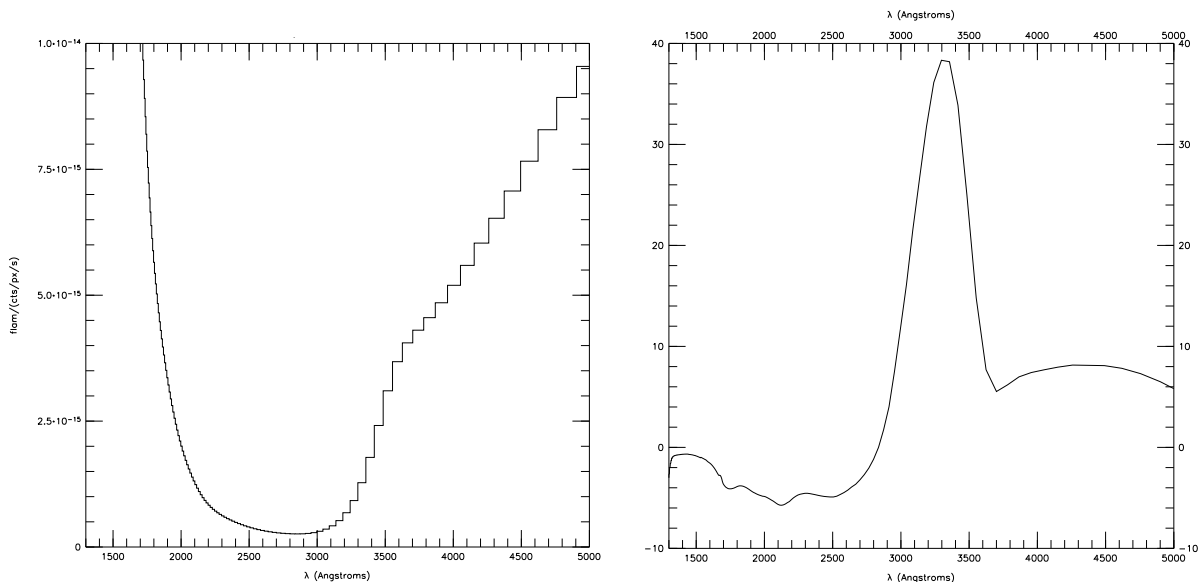


Figure 3: (left) Inverse sensitivity of the STIS objective prism with the SRF₂ filter (changes with respect to the CLEAR mode are minimal in the plotted range). A histogram is used to illustrate the variable nature of the dispersion, with each step corresponding to one pixel. (right) Percent flux error generated by shifting the location of the spectrum by one pixel in the x direction.

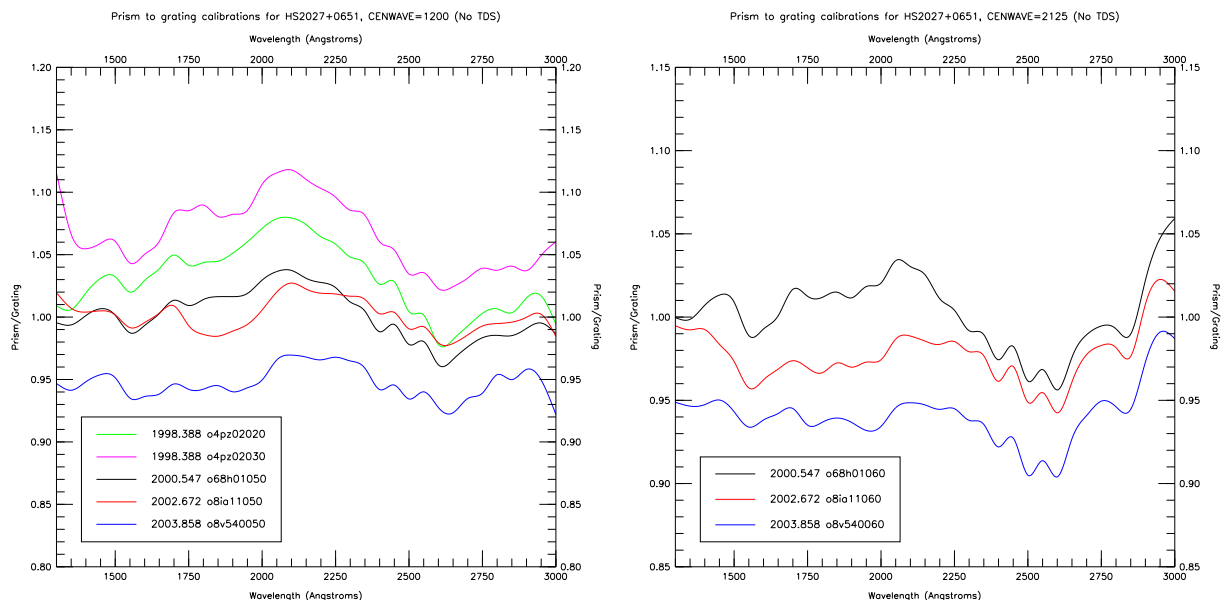


Figure 4: Ratio of the smoothed measured flux divided by the reference (grating) value for the eight datasets in our sample using the existing flux calibration. The left panel shows the five 1200 datasets and the right panel the three 2125 ones.

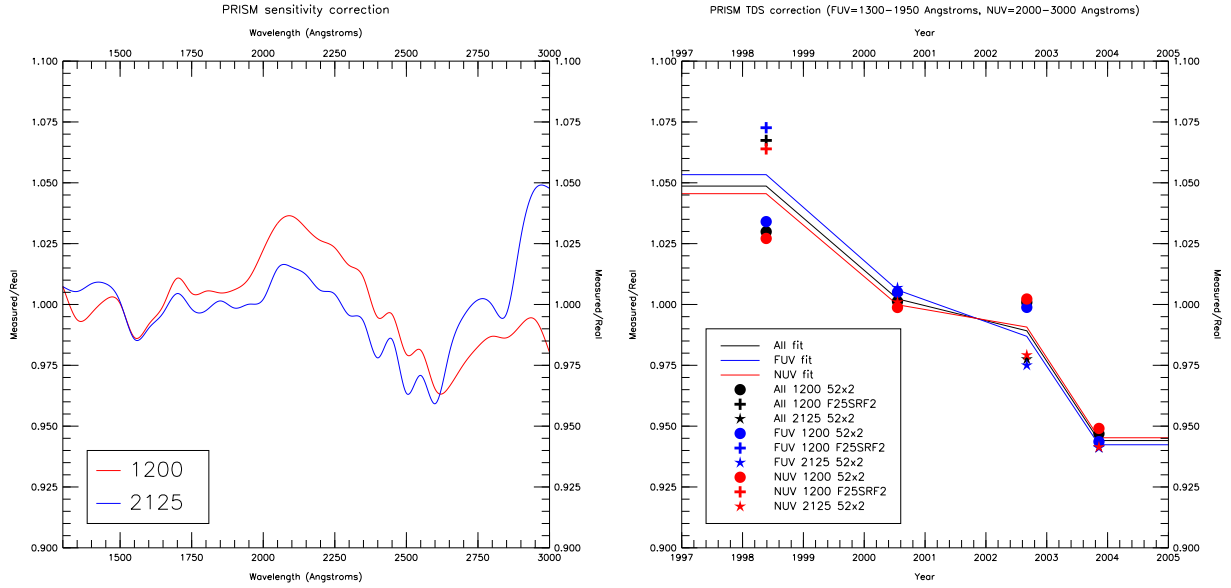


Figure 5: Sensitivity correction (left) and TDS correction (right) for the STIS objective prism derived in this ISR. The left panel shows the two independent solutions derived for each central wavelength setting. The right panel shows the solutions derived for (a) the whole wavelength range [black], (b) 1300-1950 Å [blue], and (c) 2000-3000 Å [red].

- The correction for each of the two settings can be approximately characterized by a single function of wavelength displaced by a constant which is different for each exposure.
- The corrections for the two settings also have similar relative shapes (i.e. the two functions of wavelength have similar characteristics), with a maximum around 2100 Å and a minimum around 2600 Å. However, the two curves appear not to be entirely identical.
- The displacement between each individual exposure in a setting is strongly correlated with the observation date. The sense and magnitude of the correlation with epoch appear to be similar for the two settings.

Those properties led us to devise a correction for the measured fluxes of the form $f_s(\lambda) \times g(t)$, that is, the product of a wavelength-dependent function f (different for each setting s) and a time-dependent function g . Here we will call the first part the sensitivity correction and the second one the time-dependent sensitivity (or TDS) correction. $f_s(\lambda)$ was derived by dividing each of the curves in Fig. 4 by its wavelength-averaged mean and then averaging the resulting functions. $g(t)$ was derived by interpolating in time between the wavelength-averaged means of each of the curves in Fig. 4. Results are shown in Fig. 5.

As expected from our previous impressions, the two sensitivity corrections are similar but not identical. Regarding the TDS correction, the evolution seems to be close to linear in time, with a total variation of $\approx 10\%$ between early 1998 and late 2003. We also tried to detect a possible wavelength dependence on $g(t)$, an effect which is seen for G230L data (Stys et al. 2004), by dividing our data in two ranges, “FUV” (1350-1950 Å) and “NUV” (2000-3000 Å). As seen in Fig. 5, the wavelength dependence is very weak, if present at all. Therefore,

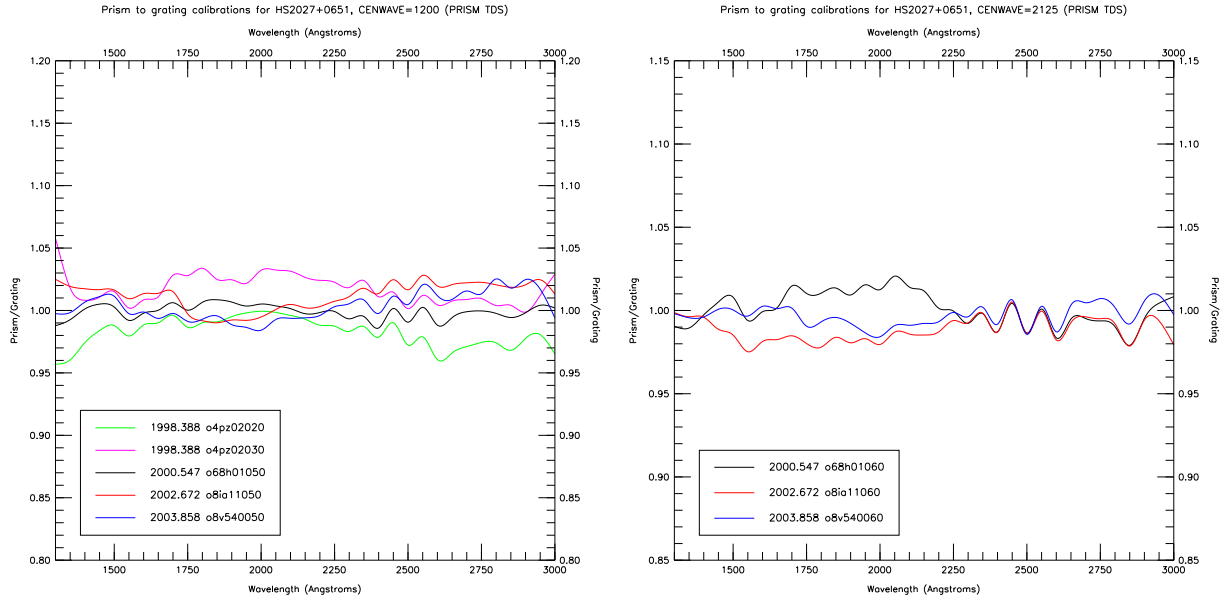


Figure 6: Same as Fig. 4 after applying the sensitivity correction and the TDS solution derived in this ISR.

we adopted a change of sensitivity with time independent of wavelength¹.

The result of applying the new sensitivity calibration is seen in Fig. 6. The rms accuracies are approximately 1% (slightly higher for the 1200 setting, slightly lower for the 2125 setting) and 90% of the data points show accuracies of 2% or better.

The TDS correction developed here has the same sign as the G230L one, and its magnitude is also comparable. At 2000 Å, the G230L TDS is quite similar to the prism one, while at 2800 Å it is $\approx 50\%$ that of the prism. We do not have enough temporal coverage to detect the rise and decline of the sensitivity that was found by Stys et al. (2004) in G230L during the first three years of operations of STIS.

$\lambda > 3000 \text{ Å}$

The STIS objective prism can detect photons in the optical band, though at a reduced sensitivity and spectral resolution (see Fig. 3 and note that it is possible to detect photons even with $\lambda > 5000 \text{ Å}$). However, two new problems are present for $\lambda > 3000 \text{ Å}$ that hamper a proper calibration of the data.

The first problem is most severe in the 3000-3500 Å range and has already been mentioned: a mismatch in the zero x position of the spectrum of 1 pixel introduces an error of a few percent at shorter wavelengths; however, it can have disastrous consequences in the 3000-3500 Å range because the slope of the sensitivity curve (as a function of pixel position, not of wavelength) is very large. As seen in the right panel of Fig. 3, the errors induced by such a small displacement can be as high as several tens of percentage points.

The second problem is severe for most of $\lambda > 3000 \text{ Å}$ and is indirectly related to the previous one. The large slope of the sensitivity curve as a function of pixel position yields large differences in the number of counts between close positions in the detector i.e. the quantity $|\text{counts}(\text{pixel a}) - \text{counts}(\text{pixel b})|/\text{distance}(\text{a,b})$

¹Due to implementation issues, the TDS correction actually implemented within the STIS pipeline correction differs slightly from the one discussed here in that the eight points in the right panel of Fig. 5 were fitted with a single straight line instead of using piecewise interpolation. This change raised the formal RMS uncertainty only very slightly (by $< 1\%$).

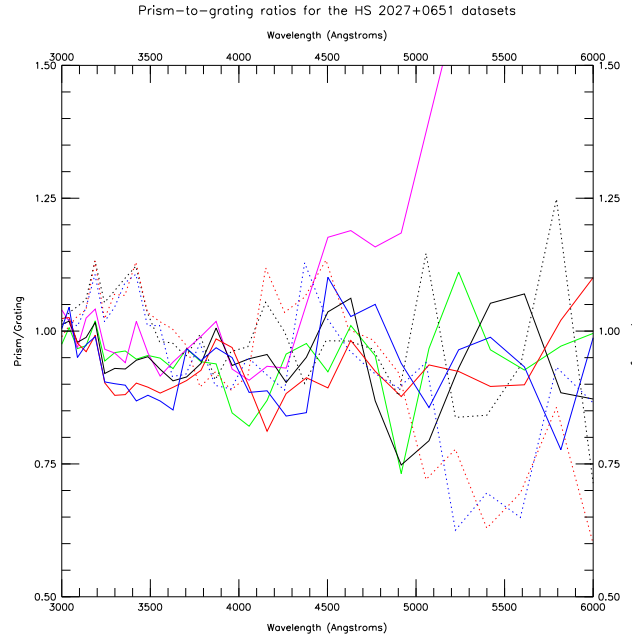


Figure 7: Prism to reference flux ratios in the 3000-6000 Å range for the eight HS 2027+0651 datasets shown in Fig. 6. The color coding is the same one as in that figure, with solid lines for the 1200 setting and dotted ones for the 2125 setting.

becomes large for small values of distance(a, b). Therefore, one expects that a significant fraction of the counts detected around e.g. 3500 Å do not originate from real photons at those wavelengths but from the wings of the line-spread function (LSF, i.e. the component of the PSF in the wavelength direction) at shorter-wavelengths (e.g. from a wavelength of 3000 Å, just a few pixels away, where the number of counts is so much higher that the wings of the LSF, parts of which fall in the pixels of the detector that correspond to 3500 Å, contain a number of counts comparable to the core of the LSF at that longer wavelength). Indeed, it can be seen that the observed cross-dispersion profile broadens considerably around 3500 Å, as expected from such LSF effects.

There is no way to precisely correct these problems, especially the latter because it arises from the intrinsic nature of the LSF. However, we devised an approximate method which consists of:

- As previously stated, using FUV lines such as Lyman α (where the spectral resolution is much better than in the NUV) to fix the zero x position of the spectrum to better than 1 pixel.
- Using the cross-dispersion profile for 3000 Å for all longer wavelengths in the MULTISPEC fit. This is done in order to minimize the artificial broadening caused by the LSF effects.
- Applying the sensitivity and TDS corrections derived in the previous subsection for $\lambda = 3000$ Å to the full optical range redward of 3000 Å.
- Adding the fit residual to the flux in the same way we did in the UV. Several values for the size of the vertical box were tested and the current default of 11 pixels turned out to give the best result.

We plot in Fig. 7 the results obtained for the eight datasets used in this ISR. In the 3000-6000 Å range, the ratio of the prism to the reference flux has a mean of 0.97 and an rms scatter of 0.13, which reflects the precision of our flux calibration in this wavelength range.

Conclusions

We have developed new photometric calibrations for the two central wavelength settings of the STIS objective prism mode. We have also calculated a wavelength-independent TDS correction specifically for the prism modes. The combination of both corrections allows for an rms accuracy of 1% with respect to the G140L+G230L results in the 1300-3000 Å range, which themselves have an absolute accuracy of 3-4% (Bohlin 2000). For $\lambda > 3000$ Å, the accuracy is lower due to imprecisions in the assignment of wavelengths to the spectrum on the detector and to contamination between adjacent wavelengths.

Acknowledgments

We would like to thank Paul Goudfrooij and Alessandra Aloisi for providing useful feedback during the review of this ISR.

Bibliography

Bohlin, R. C. 2000, *AJ* **120**, 437

Maíz-Apellániz, J. STIS ISR in preparation, “MULTISPEC: A Software for the Extraction of Slitless Spectra in Crowded Fields”.

Stys, D. J., Bohlin, R. C., and Goudfrooij, P. STIS ISR 2004-04, “Time-Dependent Sensitivity of the CCD and MAMA First-Order Modes”.